Phase Transition and Twinning Induced High Strength and Large Ductility of a Near β-Ti Alloy Processed by Double Aging

Chaoqiang Liu, Yanghuanzi Li, Song Ni, and Min Song

The mechanical properties and microstructures of a near β-Ti alloy (Ti-3.9Al-5.47Mo-4.74V-1.0Cr-1.71Fe, wt%) subjected to solution treatment and then single aging or double aging treatments were investigated by transmission electron microscopy. Single aging treatment results in an increased strength, but a decreased ductility, due to the co-precipitation of the α and ω phases or the exclusive precipitation of the α phase. Double aging breaks the strength and ductility trade-off, resulting in the highest yield strength of 1119 MPa and the largest ductility of 11%. The superior mechanical properties are ascribed to the thick α phase, FCC structure, and FCC nanotwins in the double aging treated samples.

1. Introduction

Titanium (Ti) alloys have been widely used in aerospace, chemical and biomedical industries due to their high strength to weight ratio, excellent corrosion resistance, and good biocompatibility (Ref 1). In the last few decades, near β-Ti alloys have attracted extensive attention because of their high specific strength, good processability and thermal-treatability (Ref 2). With the increasing applications of near β-Ti alloys in aviation and aerospace industries (Ref 2), such as landing gears and other structural components, improving the mechanical properties of near β-Ti alloys is of significant importance, especially the strength and the ductility.

Near β-Ti alloys usually consist of two kinds of phases, including α precipitate phase with hexagonal close-packed (HCP) structure and β matrix with body-centered cubic (BCC) structure. The α precipitate is usually the strengthening phase. The strengthening efficiency of α precipitates in near β-Ti alloys is adjustable by tailoring its size, morphology, or volume fraction through thermo-mechanical treatments (Ref 3). Additionally, ω phase is also a commonly observed phase in near β-Ti alloys, introducing which into the alloys during quenching and aging can also strengthen the alloys (Ref 4). Unfortunately, the near β-Ti alloys strengthened by α or ω phase usually present a poor ductility, which limits their wide applications. For example, according to the experimental results of Ivasishin et al. (Ref 3), the strength of a near-β Ti-5Al-5Mo-5V-1Cr-1Fe

alloy including only α strengthening phase can reach up to 1520 MPa, while its elongation is only 1.72%. A lot of previous studies have proved that some ductile alloys (such as Ti-15Mo (Ref 5), Ti-V (Ref 6), etc.) experience a ductile-to-brittle transition during aging due to the precipitation and embrittlement effect of the ω phase.

Therefore, how to develop high strength near β-Ti alloys with a desirable ductility is a significant topic of great interest. Efforts have been made on this topic by controlling the formation of α or ω phase. For example, Dong et al. (Ref 7) found that near β Ti-7Mo-3Nb-3Cr-3Al alloy can achieve a high strength and a considerable ductility using thermal treatments followed by cross-rolling, which can be ascribed to the coordination of α phases with two different morphologies, i.e., spheroidal α phase and needle-like α phase. The former is beneficial to the ductility and the latter contributes to the high strength. Gao et al. (Ref 8) reported a novel approach to obtain an ultra-high yielding strength and large strain to failure in a Ti-7Mo-3Cr-1Fe β-Ti alloy due to the addition of 1 wt% Fe, since Fe is the most efficient element to suppress the rapid growth of the brittle ω phase. Nowadays, a newly found face-centered cubic (FCC) phase in Ti alloys has attracted considerable attention. Many studies have focused on the formation mechanisms of the FCC phase (Ref 9, 10), the twinning behavior of the FCC phase (Ref 11) and its influence on the mechanical properties (Ref 12, 13) due to its good deformability. In our previous study, we found that the FCC phase generated during hot rolling process plays an important role in the subsequent tensile deformation of a near β Ti alloy and is responsible for the high strength and large ductility of the alloy (Ref 13).

In this paper, a near β-Ti-45512 alloy was solution heat treated, and then aged to different conditions to control the precipitates. We found that the strength and ductility trade-off dilemma can be overcome in this alloy by double aging, and a near β Ti-45512 alloy with high strength and good ductility was developed. Moreover, the microstructures in the alloy under different heat treatment conditions were also examined and the relationships between microstructures and mechanical properties were discussed.

Chaoqiang Liu and Yanghuanzi Li have contributed equally to this work.

Chaoqiang Liu, Yanghuanzi Li, Song Ni, and **Min Song**, State Key Laboratory of Powder Metallurgy, Central South University, Changsha 410083, China. Contact e-mail: msong@csu.edu.cn.

2. Material and Methods

The chemical composition of the near β-Ti-45512 alloy in the present study was measured to be Ti-3.9Al-5.47Mo-4.74V-1.0Cr-1.71Fe (wt%). The β-transus temperature of this alloy is approximately 875 °C by using the metallographic method. The as-received Ti-45512 ingots were sectioned into small samples with a dimension of 30 × 20 × 10 mm. All of the as-received samples were firstly solution-treated at 900 °C for 0.5 h, followed by air quenching (designated as AQ samples). Subsequently, some AQ samples were directly aged at 400 °C for 8 h (designated as SA1 samples) or 16 (designated as SA2 samples), and some other AQ samples were firstly aged at 400 °C for 15 h, then heated to 600 °C and kept for 1 h (designated as DA sample). All specimens were subjected to tensile experiments in an Instron 3369 machine at the room temperature with a strain rate of 0.001 s^{-1}. The tensile specimen has a gauge length of 8 mm, and a cross section of 3.4 × 2 mm. For each condition, three samples were tested to ensure the validity of the tensile data. X-ray diffraction (XRD, D/max2550pc x-ray diffractometer) was used to examine phase constitutions of the samples. Microstructures of the different samples were characterized by transmission electron microscopy (TEM) in FEI Tecnai G^2 F20 and FEI Titan G^2 60-300 microscopes. Specimens for TEM observations were prepared by firstly mechanically grinding and then electro-polishing in a solution of 5% HClO$_4$, 35% CH$_3$(CH$_2$)$_3$OH, and 60% CH$_3$OH at −30 °C.

3. Results and Discussion

Figure 1(a) shows the tensile engineering stress-engineering strain curves of AQ, SA1, SA2 and DA samples. The AQ sample has the lowest yield strength of about 714 MPa and a low ductility of about 2.2%, as shown in Table 1. The possible reasons for the low ductility of AQ sample may be caused by the three possible reasons: (1) a fast-cooling velocity might introduce internal friction in the matrix, (2) the formation of very tiny adiabat phase, which cannot be determined by traditional TEM images or SEAD pattern due to its small size

and volume fraction, and (3) multiple alloying elements dissolved in the β phase may introduce a large lattice torsion and confine the dislocation gliding. After aging treatment at 400 °C, the alloy is strengthened dramatically. The SA1 and SA2 samples exhibit a superior tensile yield strength of ∼998 MPa and ∼1109 MPa, respectively. But with the increase in their strength, the ductility becomes much lower. This is expected since strength and ductility trade-off occurs commonly in metallic materials. Unexpectedly, when the alloy was aged initially at 400 °C for 15 h and then at 600 °C for 1 h, its strength and ductility increase simultaneously. The DA samples present the highest tensile yield strength of ∼1119 MPa and the largest elongation to fracture of ∼11.1%. Note that the AQ sample has the lowest elastic modulus compared to the others. Fig. 1(b) shows the aging hardening curve of the AQ sample at 400 °C. The sample has a desirable aging hardening response when it aged at 400 °C. The hardness value of the SA1 and SA2 samples are 537 HV and 539 HV, respectively, while the hardness value is 502 HV for the DA sample, as shown in Table 1.

In order to reveal the underlying mechanisms of tensile properties variation during aging processes, microstructures in different heat-treated samples were characterized. Figs. 2(a-c) show a bright field (BF) TEM image and corresponding selected area electron diffraction (SAED) patterns of AQ samples along [011]$_β$ and [$\bar{1}$11]$_β$ zone axes, respectively. The BF image has a uniform contrast and these two SAED patterns include no extra diffraction spots except for those of the β-Ti matrix, which indicates that the AQ samples only include single β solid solution. This is further demonstrated by the XRD

Table 1 Tensile properties and hardness of different samples

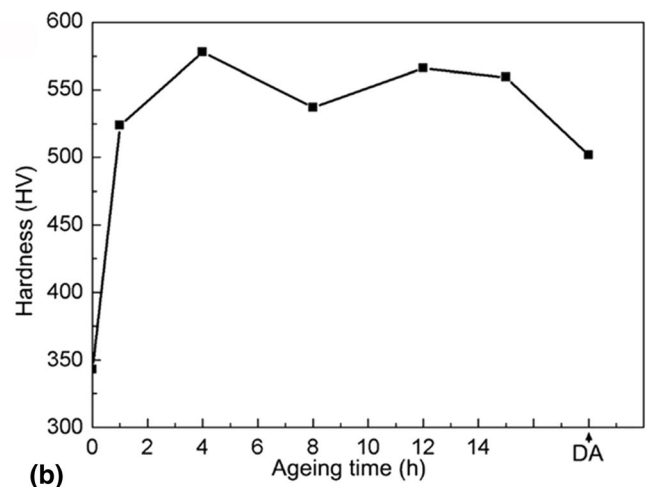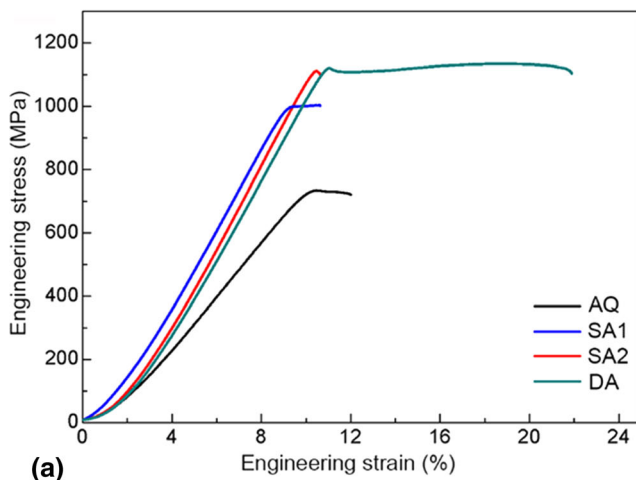|	YTS, MPa	UTS, MPa	El, %	Hardness, HV
AQ	714	734	2.2	343
SA1	998	1004	1.5	537
SA2	1109	1112	0.6	539
DA	1119	1134	11.1	502

(a)

(b)

Fig. 1 (a) Engineering stress-engineering strain curves showing the tensile properties of the samples in different heat treatment conditions, (b) aging hardening curve of AQ sample aged at 400 °C
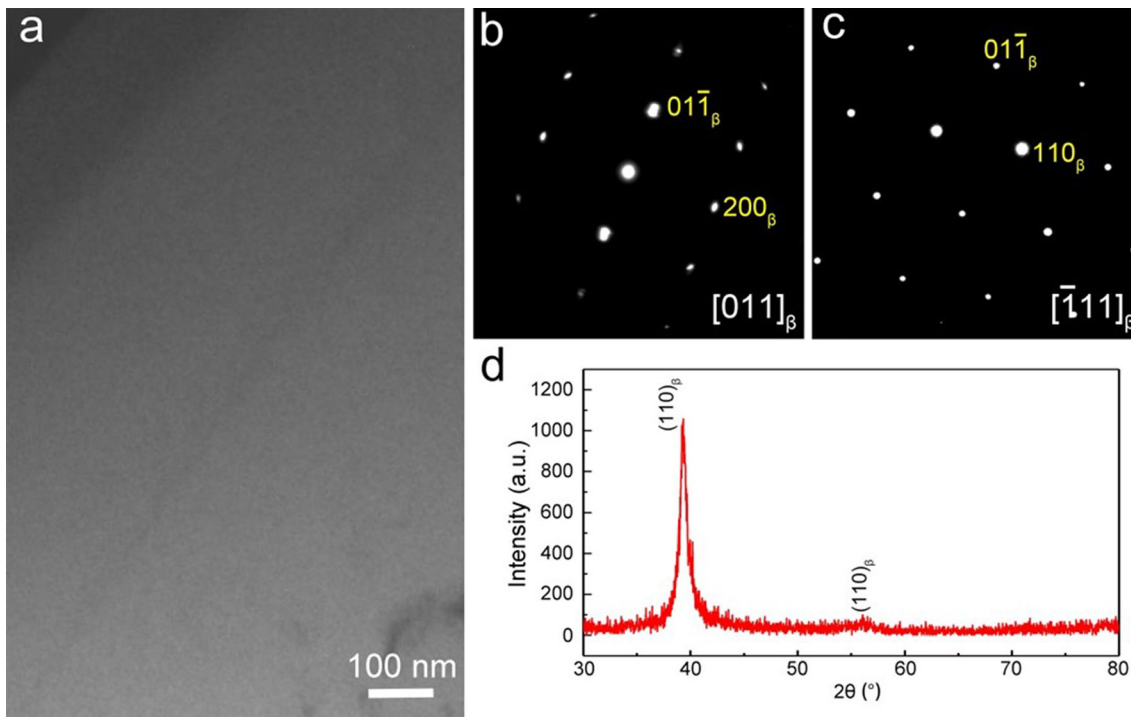
Fig. 2 (a) BF-TEM image, (b, c) SAED patterns recorded along [011] and [$\bar{1}$11] zone axes in AQ sample, and (d) XRD pattern of an AQ sample

pattern of an AQ sample in Fig. 2(d). The XRD pattern includes exclusively the x-ray diffraction peaks of the β-Ti matrix.

Figure 3(a) shows a BF-TEM image in a SA1 sample along $[011]_\beta$ zone axis. In contrast to the AQ samples, the SA1 sample includes acicular α precipitates marked by the arrows and dispersive ω precipitates marked by the ellipse in Fig. 3(a). The α precipitates are at 90° to each other and approximately 100 nm in length viewed from this direction. Fig. 3(b) shows the corresponding SAED pattern of the SA1 sample. Apart from the diffraction spots of the β-Ti matrix, the diffraction spots of two α variants and ω phase were detected. Through indexing the diffraction patterns, the orientation relationship (OR) between α precipitates and β-Ti matrix is such that $[1\bar{2}10]_\alpha$ // $[\bar{1}11]_\beta$ and $(0001)_\alpha$ // $(110)_\beta$. This OR is the typical Burgers OR, which has been widely reported in the previous studies (Ref 14-17). Although the Burgers OR leads to 12 crystallographic variants (Ref 17, 18), only two of them are exactly on $[0001]_\alpha$ zone axis for a given $[110]_\beta$ direction. Fig. 3(c) and (d) show a BF-TEM image and the corresponding SAED pattern along $[011]_\beta$ zone axis in a SA2 sample, respectively. In this sample, the α precipitates are still at 90° to each other marked by arrows in Fig. 3(c) and grow to a plate-like morphology, when they are viewed from $[011]_\beta$ direction. The OR between α precipitate and β-Ti matrix is still the Burgers OR. In contrast, no ω precipitate was detected in this SA2 specimen, as shown in Fig. 3(d).

Figure 4(a) shows the microstructure in a DA sample. This sample is consisted of β-Ti matrix and lamellar α phase. The size of these α lamellae is 200-500 nm in length and 50-200 nm in thickness, which is much larger than that of α aciculae in SA1 specimens and that of α plates in SA2 samples. Fig. 4(b) shows the enlarged microstructure in the DA sample. Interestingly, many equiaxial particles, distributed inside the β-Ti matrix, near the β/α interface, or in the α precipitate, are

observed, and some of them are marked by dashed circles in Fig. 4(b). In order to determine the structure of these particles, one of them was further enlarged in Fig. 4(c). The inset in Fig. 4(c) is its corresponding SAED pattern. According to the SAED pattern, the particle is identified as FCC structure, and contains nanotwins in it. The twinning plane is determined to be $(11\bar{1})$ plane. Fig. 4(d) shows the high-resolution TEM (HRTEM) image of an FCC particle inside the β-Ti matrix. The inverse fast Fourier-filtered (IFFT) images of the β-Ti matrix and the FCC structures are inserted in Fig. 4(d). The FFT pattern of this HRTEM image is displayed in the upper right corner of the image, showing clearly the coexistence of the β-Ti matrix, FCC structures and its twins. According to the FFT pattern, the OR between the β-Ti matrix and the FCC structures can be determined as $(110)_\beta$ // $(\bar{1}11)_{FCC}$ and $[\bar{1}11]_\beta$ // $[110]_{FCC}$. Based on the Burgers OR between the β-Ti matrix and the α phase, the OR between the α phase and the FCC structure can be speculated to be $(0001)_\alpha$ // $(\bar{1}11)_{FCC}$ and $[1\bar{2}10]_\alpha$ // $[110]_{FCC}$, which is consistent with the previous reports (Ref 12, 13). In order to further characterize the FCC structure and its twins, an area marked roughly by white dashed frame in Fig. 4(d) is enlarged slightly and shown in Fig. 4(e). Three inserted FFT images are obtained from different areas marked A, B, and C in Fig. 4(e). FFT-A indicates that region-A is FCC structure while FFT-B indicates region-B is also FCC structure but with different orientation. FFT-C was acquired in the interface between these two FCC structures, suggesting an obvious twin relationship. The twin boundary (TB) is clearly shown in the inserted IFFT image in Fig. 4(e). Along this twin boundary, there is no lattice distortion and misfit dislocation, indicating the coherency.

The formation of the FCC structure in Ti and its alloys has been widely observed in previous studies (Ref 11, 13, 19). It is different from Ti-hydride as the hydride has a lath or needle
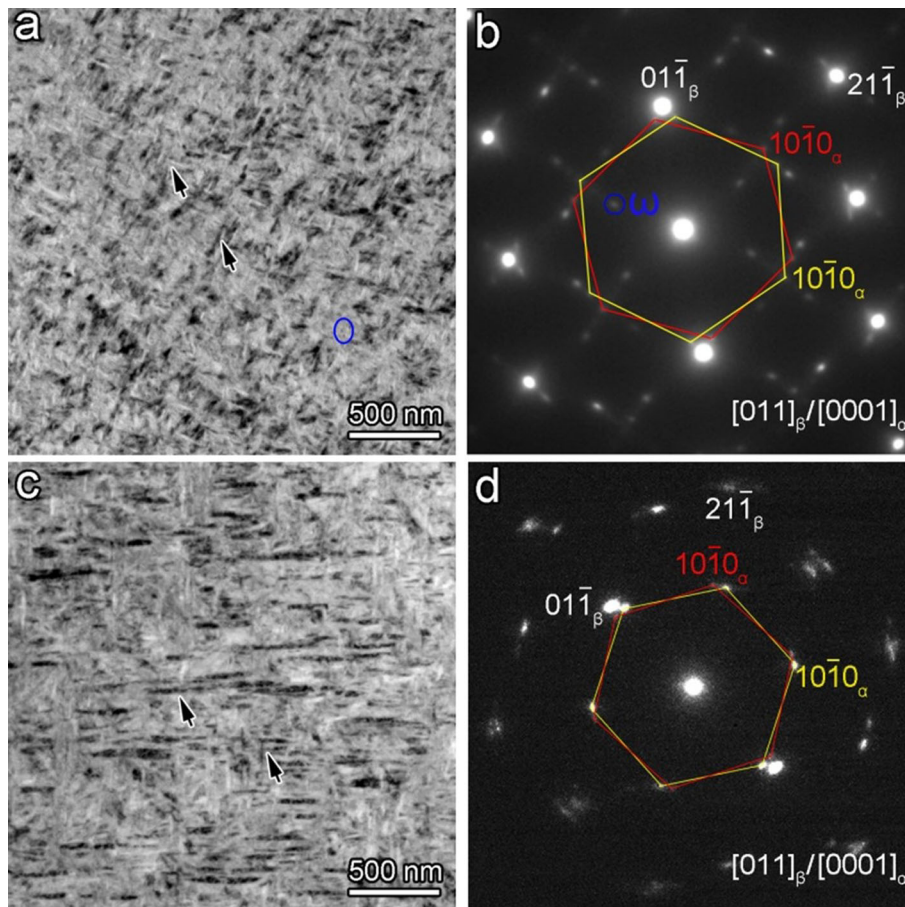
Fig. 3 (a, c) BF-TEM images and (b, d) SAED patterns showing the microstructures in SA1 and SA2 samples, respectively. The arrows in (a) and (c) indicate α precipitates and the small blue ellipse in (a) marks ω phase

morphology (Ref 20, 21) and similar FCC structures were observed in specimens prepared by focused ion beam in our previous study (Ref 13). This FCC structure is formed by HCP to FCC transformation. It has been reported that this transformation occurs during heat treatment (Ref 19, 22) or plastic deformation (Ref 9, 10). The formation of this FCC structure involves the generation and movement of Shockley partial dislocations on the basal plane of the α phase (Ref 23, 24). In addition, twinning is one kind of commonly observed deformation mode in the alloys with FCC structure (Ref 25). However, in this study, twins are detected frequently in DA samples that were not subjected to deformation. Thus, these FCC twins cannot be produced by deformation. They might be the twin-related variants of the FCC structure. Fig. 5(b) illustrates schematically two twin-related FCC variants transformed from a HCP structure in Fig. 5(a). The cause of the generation of twin-related variants is that this configuration of two FCC variants can lead the stains introduced by the formation of these two FCC variants to accommodate each other, and then decrease the total energy. Similar phenomenon has been reported in previous studies (Ref 23, 24).

Figure 6 shows the fractographs of AQ, SA1, SA2, and DA samples. The fracture microstructure of the AQ sample is consisted of cleavage faces and shallow dimples. The cleavage faces are relatively large in area and dimples is located at the border of the cleavage faces. Similarly, the fracture microstructure of the SA1 and SA2 samples are also comprised of cleavage faces and dimples, although their size and distribution are different. In contrast, the DA sample has a totally different fracture microstructure, as shown in Fig. 6(d) and (h). No obvious cleavage face is observed in its fracture surface and its fracture microstructure is dominated by dimples. In addition, some dimples are relatively deep. This kind of fracture microstructure implies that the DA sample has a good ductility in comparison with AQ, SA1, and SA2 samples, which is consistent with the tensile results in Fig. 1(a).

It has been shown from Fig. 1(a) that the AQ samples including single β-Ti phase have the lowest tensile strength. This is reasonable because all of the alloying elements in the AQ sample were dissolved into the β-Ti matrix, and the strengthening mechanism in the AQ sample is mainly solid solution strengthening. When the AQ samples were aged at 400 °C for 8 h, acicular α phases and ω phases precipitate out from the β-Ti matrix, as shown in Figs. 3(a-b). The α/β interfaces and the ω/β interfaces would act as dislocation barriers and impede strongly the dislocation gliding (Ref 26–28), which leads to the improvement of the strength. Further increasing the aging time would makes the ω phase act as heterogeneous nucleation site for the α precipitate nucleation (Ref 29, 30), which would further increase the number density of the α precipitates. This might be the reason why the SA2 samples have a higher strength than the SA1 samples. Although the precipitation of α and ω phases result in the enhanced strength, they severely limit the dislocation movements, and then cause
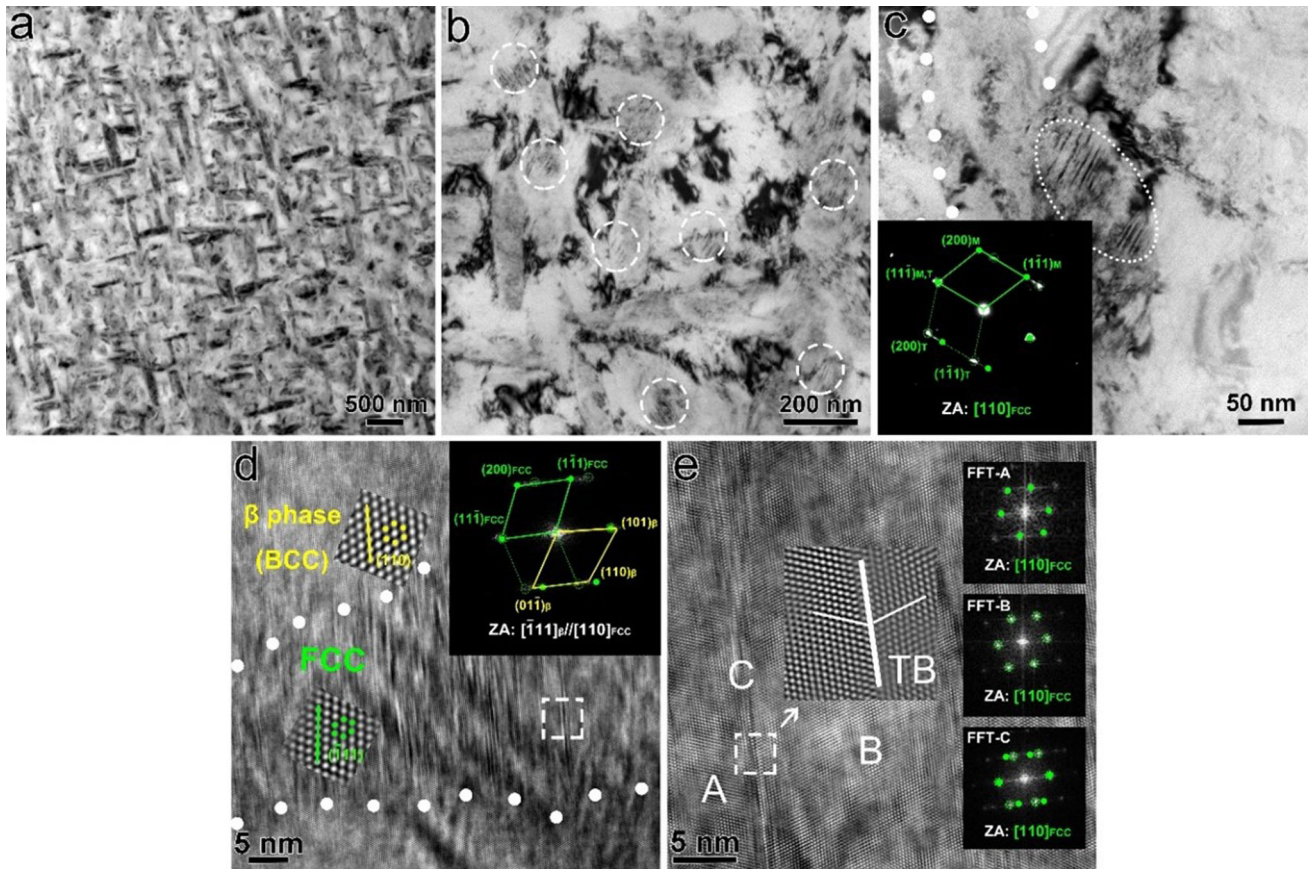
Fig. 4 (a-c) BF-TEM and (d, e) HRTEM images showing the microstructure in a DA sample. The inset in the left bottom corner of (c) is SAED pattern of an FCC particle. The inset in the right upper corner of (d) is the corresponding FFT pattern of (d)
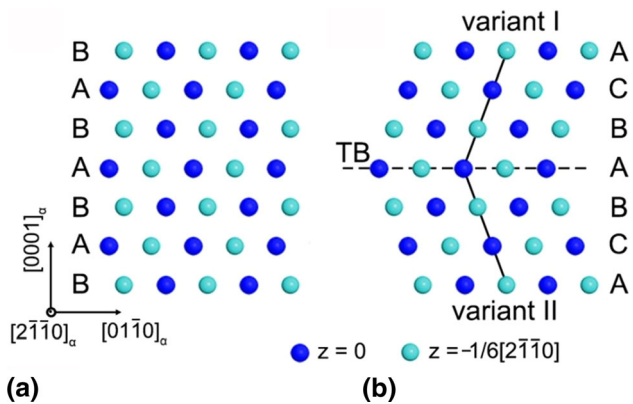

Fig. 5 Schematic diagram showing (a) an HCP structure and (b) two twin-related FCC variants formed from the HCP structure

grown significantly, even some of them are equiaxed, compared to those in the SA1 and SA2 samples, as shown in Fig. 3 and 4, their precipitation strengthening effect decreases dramatically. Therefore, the high strength of the DA samples should be attributed to the densely distributed FCC structure and the nanotwins inside the FCC structure. The FCC structures can impede the dislocation gliding and the twin boundaries can also act as obstructions for dislocation movements as the ω/β and α/β interfaces to achieve strength enhancements. Previous studies have reported that nanotwins in FCC structures can result in high strength (Ref 31, 32). In addition to providing the desirable strengthening effect, these FCC structures containing nanotwins can also improve the ductility of the alloy (Ref 13, 31), since they not only have more available slip systems, but they can also transform back to the HCP structure during deformation. Apart from the contribution of the FCC structure to the ductility of the DA alloy, the thick α lamellae, especially those near equiaxial α phases, are also responsible to the superior ductility since they shows good compatibility during deformation (Ref 33). It has been reported that the unique dislocation patterns exist in the samples including α phase with equiaxial structure, such as dislocation channel structures and shear bands, and that equiaxial α-Ti phase can provide effective glide for mobile dislocations, thus resulting in a good ductility (Ref 34).
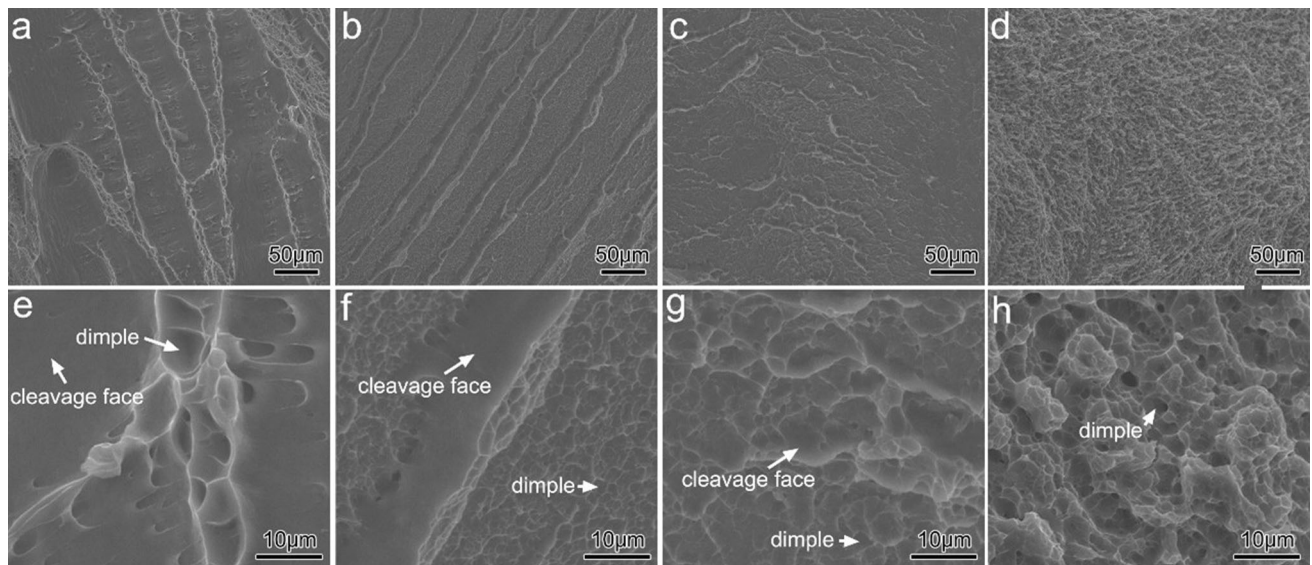
early cracking of the samples during deformation. This explains that the SA1 and SA2 samples have a low ductility. With regarded to the lowest elastic modulus of the AQ sample, which is due to the fact that β phase has a lower elastic modulus than α phase in titanium alloys and precipitation of α phase from β solid solution would lead to an increased elastic modulus of the alloy.

When the AQ samples were initially aged at 400 °C for 15 h and then at 600 °C for 1 h, the samples have not only the highest strength, but also the best ductility, as shown in Fig. 1(a). Since the α precipitates in the DA samples have

Fig. 6. SEM images showing (a-d) low-magnification and (e-h) high-magnification fractographs of (a, e) AQ, (b, f) SA1, (c, g) SA2, and (d, h) DA samples

4. Conclusions

In summary, a near β-Ti-45512 alloy was solution and then aging treated in this study. The mechanical properties and microstructures of the samples under different heat-treated conditions were investigated. The tensile yield strength of the solutionized sample is increased from 714 MPa to 998 MPa or 1113 MPa after aging treatment at 400 °C for 8 h (SA1) or 16 h (SA2), but its ductility is decreased. The SA1 samples include fine acicular α precipitate and dispersive ω precipitate, and the SA2 samples include only plate-like α precipitate. When the solutionized sample was firstly aged at 400 °C for 15 h and then 600 °C for 1 h (DA), its strength and ductility are increased simultaneously. The DA samples reach to the highest yield strength of 1119 MPa and the largest ductility of ∼11%. The high strength and large ductility are attributed to the thick α phase, FCC structure, and FCC nanotwins.

References

1. D. Banerjee and J.C. Williams, Perspectives on Titanium Science and Technology, *Acta Mater.*, 2013, **61**, p 844–879
2. J.D. Cotton, R.D. Briggs, R.R. Boyer, S. Tamirisakandala, P. Russo, N. Shchetnikov and J.C. Fanning, State of the Art in Beta Titanium Alloys for Airframe Applications, *JOM*, 2015, **67**, p 1281–1303
3. O.M. Ivasishin, P.E. Markovsky, Y.V. Matviychuk, S.L. Semiatin, C.H. Ward and S. Fox, A Comparative Study of the Mechanical Properties of High-Strength β-Titanium Alloys, *J. Alloys Comp.*, 2008, **457**, p 296–309
4. J.C. Williams, B.S. Hickman and H.L. Marcus, The Effect of Omega Phase on the Mechanical Properties of Titanium Alloys, *Matall. Trans.*, 1971, **2**, p 1913–1919
5. A.W. Bowen, Omega Phase Embrittlement in Aged Ti-15%Mo, *Scr. Metall.*, 1971, **5**, p 709–715
6. M.K. Koul and J.F. Breedis, Omega Phase Embrittlement in Aged Ti-V, *Metall. Mater. Trans.*, 1970, **1**, p 1451–1452
7. R. Dong, J. Li, H. Kou, J. Fan and B. Tang, Dependence of Mechanical Properties on the Microstructure Characteristics of a near β Titanium Alloy Ti-7333, *J. Mater. Sci. Technol.*, 2019, **35**, p 48–54
8. J. Gao, A.J. Knowles, D. Guan and W.M. Rainforth, ω Phase Strengthened 1.2GPa Metastable β Titanium Alloy with High Ductility, *Scr. Mater.*, 2019, **162**, p 77–81
9. H.C. Wu, A. Kumar, J. Wang, X.F. Bi, C.N. Tomé, Z. Zhang and S.X. Mao, Rolling-Induced Face Centered Cubic Titanium in Hexagonal Close Packed Titanium at Room Temperature, *Sci. Rep.*, 2016, **6**, p 24370
10. D.H. Hong, T.W. Lee, S.H. Lim, W.Y. Kim and S.K. Hwang, Stress-Induced Hexagonal Close-Packed to Face-Centered Cubic Phase Transformation in Commercial-Purity Titanium under Cryogenic Plane-Strain Compression, *Scr. Mater.*, 2013, **69**, p 405–408
11. Y.G. Liu, M.Q. Li and H.J. Liu, Deformation Induced Face-Centered Cubic Titanium and its Twinning Behavior in Ti-6Al-4V, *Scr. Mater.*, 2016, **119**, p 5–8
12. N. Ao, D. Liu, C. Liu, X. Zhang and D. Liu, Face-Centered Titanium Induced by Ultrasonic Surface Rolling Process in Ti-6Al-4V Alloy and its Tensile Behavior, *Mater. Charact.*, 2018, **145**, p 527–533
13. Y. Li, S. Ni, Y. Liu and M. Song, Phase Transition Induced High Strength and Large Ductility of a Hot Rolled near β Ti-5Al-5Mo-5V-1Cr-1Fe Alloy, *Scr. Mater.*, 2019, **170**, p 34–37
14. Y.M. Zhu, S.M. Zhu, M.S. Dargusch and J.F. Nie, HAADF-STEM Study of Phase Separation and the Subsequent α Phase Precipitation in a β-Ti Alloy, *Scr. Mater.*, 2016, **112**, p 46–49
15. T. Furuhara, T. Makino, Y. Idei, H. Ishigaki, A. Takada and T. Maki, Morphology and Crystallography of α Precipitates in β Ti-Mo Binary Alloys, *Mater. Trans.*, 1998, **39**, p 31–39
16. F. Ye, W.Z. Zhang and D. Qiu, A TEM Study of the Habit Plane Structure of Intragrainular Proeutectoid α Precipitates in a Ti-7.26 wt%Cr Alloy, *Acta Mater.*, 2004, **52**, p 2449–2460
17. S. Balachandran, A. Kashiwar, A. Choudhury, D. Banerjee, R. Shi and Y. Wang, On Variant Distribution and Coarsening Behavior of the α Phase in a Metastable β Titanium Alloyoy, *Acta Mater.*, 2016, **106**, p 374–387
18. S.C. Wang, M. Aindow and M.J. Starink, Effect of Self-Accommodation on α/α Boundary Populations in Pure Titanium, *Acta Mater.*, 2003, **51**, p 2485–2503
19. Q. Yu, J. Kacher, C. Gammer, R. Traylor, A. Samanta, Z. Yang and A.M. Minor, In situ TEM Observation of FCC Ti Formation at Elevated Temperaturess, *Scr. Mater.*, 2017, **140**, p 9–12

20. Y. Chang, S. Zhang, C.H. Liebscher, D. Dye, D. Ponge, C. Scheu, G. Dehm, D. Raabe, B. Gault and W. Lu, Could Face-Centered Cubic Titanium in Cold-Rolled Commercially-Pure Titanium only be a Ti-Hydride?, *Scr. Mater.*, 2020, **178**, p 39–43

21. E. Conforto and D. Caillard, A Fast Method for Determining Favourable Orientation Relationships and Interface Planes: Application to Titanium-Titanium Hydrides Transformations, *Acta Mater.*, 2007, **55**, p 785–798

22. R. Jing, C.Y. Liu, M.Z. Ma and R.P. Liu, Microstructural Evolution and Formation Mechanism of FCC Titanium During Heat Treatment Processing, *J Alloys Comp.*, 2013, **552**, p 202–207

23. H. Zhao, M. Song, S. Ni, S. Shao, J. Wang and X. Liao, Atomic-Scale Understanding of Stress-Induced Phase Transformation in Cold-Rolled Hf, *Acta Mater.*, 2017, **131**, p 271–279

24. C.Q. Liu, H.W. Chen, H. Liu, X.J. Zhao and J.F. Nie, Metastable Precipitate Phases in Mg-9.8wt%Sn Alloy, *Acta Mater.*, 2018, **144**, p 590–600

25. L. Wang, P. Guan, J. Teng, P. Liu, D. Chen, W. Xie, D. Kong, S. Zhang, T. Zhu, Z. Zhang, E. Ma, M. Chen and X. Han, New Twinning Route in Face-Centered Cubic Nanocrystalline Metalss, *Nat. Commun.*, 2017, **8**, p 2142

26. C. Huang, Y. Zhao, S. Xin, W. Zhou, Q. Li and W. Zeng, Effect of Microstructure on Tensile Properties of Ti-5Al-5Mo-5V-3Cr-1Zr Alloyy, *J. Alloys Comp.*, 2017, **693**, p 582–591

27. F. Sun, J.Y. Zhang, P. Vermaut, D. Choudhuri, T. Alam, S.A. Mantri, P. Svec, T. Gloriant, P.J. Jacques, R. Banerjee and F. Prima, Strengthening Strategy for a Ductile Metastable β-Titanium Alloy using Low-Temperature Aging, *Mater. Res. Lett.*, 2017, **5**, p 547–553

28. W. Kou, Q. Sun, L. Xiao and J. Sun, Coupling Effect of Second Phase and Phase Interface on Deformation Behaviours in Microscale Ti-55531 Pillars, *J. Alloys Comp.*, 2020, **820**, p 153421

29. Y. Zheng, R.E.A. Williams, D. Wang, R. Shi, S. Nag, P. Kami, J.M. Sosa, R. Banerjee, Y. Wang and H.L. Fraser, Role of ω Phase in the Formation of Extremely Refined Intragranular α Precipitates in Metastable β-Titanium Alloys, *Acta Mater.*, 2016, **103**, p 850–858

30. R. Shi, Y. Zheng, R. Banerjee, H.L. Fraser and Y. Wang, ω-Assisted α Nucleation in a Metastable β Titanium Alloy, *Scr. Mater.*, 2019, **171**, p 62–66

31. K. Lu, L. Lu and S. Suresh, Strengthening Materials by Engineering Coherent Internal Boundaries at the Nanoscale, *Science*, 2009, **324**, p 349–352

32. L. Lu, Y. Shen, X. Chen, L. Qian and K. Lu, Ultrahigh Strength and High Electrical Conductivity in Copper, *Science*, 2004, **304**, p 422–426

33. J. Huang, Z. Wang and K. Xue, Cyclic Deformation Response and Micromechanisms of Ti Alloy Ti-5Al-5V-5Mo-3Cr-0.5Fe, *Mater. Sci. Eng. A*, 2011, **528**, p 8723–8732

34. Z. Zhao, J. Chen, H. Tan, G. Zhang, X. Lin and W. Huang, Achieving Superior Ductility for Laser Solid Formed Extra Low Interstitial Ti-6Al-4V Titanium Alloy Through Equiaxial Alpha Microstructuree, *Scr. Mater.*, 2018, **146**, p 187–191